Single-Cell Detection Using Optofluidic Intracavity Spectroscopy

Hua Shao, *Student Member, IEEE*, Dhiraj Kumar, *Student Member, IEEE*, and Kevin L. Lear, *Member, IEEE*

***Abstract*—Optofluidic intracavity spectroscopy was used to realize label-free detection of single biological cells, including yeast cells and human blood cells, as well as polystyrene spheres in a microfluidic Fabry–Perot cavity. The design, fabrication, and testing of the cavities are discussed, along with the sensing mechanism. The resonant conditions of the microfluidic cavity were modified by the cells and microspheres inside the cavity due to the effective refractive index profile of the cells. Transmission spectra of single cells in the cavity, measured using a customized microscope system, exhibited cell-type specific higher order transverse mode features, including the number of transverse modes, mode shape, and the relative mode spacing. A correlation method for the cell-induced spectra is reported and provides a preliminary demonstration that some types of single cells can be differentiated. After further development, the method may provide a useful label-free optical technique for recognizing cells in a microfluidic environment.**

***Index Terms*—Biological cell differentiation, intracavity spectroscopy, microfluidic cavity, transmission spectra, transverse mode.**

I. Introduction

LOW COST and label-free detection of single biological cells is of broad interest in a variety of fields, including clinical diagnostics, drug discovery, food safety, environmental monitoring, biology, and homeland security. Cell detection, identification, and monitoring are important capabilities for these applications. Cell parameters including size, shape, and refractive index profile provide substantial information about the presence and state of particular cells [1]. Automated sensing of these parameters directly or indirectly, either individually or in combination, can improve current methods. For example, simple whole blood counts are a relatively straightforward task, but the traditional method requires staining and microscopic examination. A lab-on-a-chip automated sensor that could perform this task without staining or labeling in a point-of-care environment would clearly be useful, yet it would only need to detect and differentiate among a small set of cell types such as red and white blood cells (WBCs). More sophisticated monitoring of morphological or optical changes can be used to track the state of cell populations or indicate an inflammatory response of biological tissues. For example, the enlargement of the cell nuclei has been used as a primary indicator of cancer in most human tissues [2]. Beside nuclei enlargement, cancer cells have higher effective refractive indexes than normal cells due to the larger refractive index of the chromatin contents in the nuclei than that of the surrounding cytoplasm [1].

Optical processes such as light scattering, absorption, and diffraction can be used for the detection of single cells. Techniques ranging from direct imaging methods, such as autofluorescence [3] and confocal microscopy [4], to spectroscopic methods, such as confocal Raman [5], scattering [6], and cavity ring-down spectroscopy [7], have been used to detect single biological cells. However, each approach has its own advantages and disadvantages. For example, light-scattering spectroscopy provides noninvasive measurements of the size, shape, and refractive index of the cell [8], but the associated optical experimental setup and data analysis are complicated and expensive due to the angular dependence of the scattered light. Similar problems exist in the Raman spectroscopic system [5], which typically requires moderate to high-power lasers as well as various optical filters to remove the interferences of the excitation source and intrinsic fluorescence of the cells. Conventional methods, such as fluorescence spectroscopy, require time and reagent consuming fluorescent labeling processes to enhance the signal to noise ratio. Although autofluorescence microscopy without any sample labeling has been investigated, it is mainly limited to cells with a strong autofluorescent signal [3]. Issues such as the need for biorecognition coatings to obtain sufficient sensitivity for single-cell detection may impact cavity ring-down spectroscopy [7]. Given the limitations of existing single-cell sensor technology, evaluating the utility of new approaches and issues surrounding their performance continues to be of interest.

The concept of optofluidic intracavity spectroscopy (OFIS) reported in this paper utilizes optical refraction and diffraction effects in cells to produce characteristic intracavity transmission spectra of single biological cells in an optical resonator. Biological samples such as cells, DNA, protein layers, or biological fluids placed inside an optofluidic cavity modify the resonant conditions of the cavity, providing a probe to detect the biological samples. Many optical cavity or optical resonator related sensors are based on the observation of longitudinal mode shifts rather than the transverse mode formation discussed below. Longitudinal shifts may require high-resolution spectrometry (< 0.1 nm) in order to provide adequate sensitivity [9].

Manuscript received January 10, 2006; revised March 7, 2006. This work was supported in part by the Defense Advanced Research Projects Agency (DARPA) under Research Contract E-21-F89-G1. The associate editor coordinating the review of this paper and approving it for publication was Prof. Eugenii Katz.

H. Shao and K. L. Lear are with the Electrical and Computer Engineering Department, Colorado State University, Fort Collins, CO 80523 USA (e-mail: lshao@engr.colostate.edu; kllear@engr.colostate.edu).

D. Kumar was with the Electrical and Computer Engineering Department, Colorado State University, Fort Collins, CO 80523 USA. He is now with the Opticomp Corporation, Zephyr Cove, NV 89448 USA (e-mail: kumar.dhiraj@gmail.com).

Color versions of all figures are available online at http://ieeexplore.ieee.org.
Digital Object Identifier 10.1109/JSEN.2006.884512

Environmental factors, such as temperature-induced refractive index changes, may also impact the sensitivity of high-Q-factor resonant systems relying on longitudinal mode shifts of optical cavities [10]. In contrast, the sensing mechanism presented here relies on the relative relationship between transverse modes formed in microfluidic Fabry–Perot (FP) cavities induced by transverse variation in the optical thickness of cells related to their size, shape, and composition. Temperature changes affect the transverse mode spacing much less than the absolute wavelength of longitudinal modes. Further, the transverse mode spacing is often $>$ 0.1 nm, which allows lower resolution spectrometry. The mechanism for transverse mode formation is discussed in greater detail in Section II.

Previous work on transverse mode-based intracavity spectroscopy of single biological cells inside the resonator of an optically pumped vertical extended cavity surface-emitting laser (VECSEL) was reported by Gourley, who referred to their device as a biocavity laser [11]. They demonstrated that different cell types resulted in multimode laser spectra with mode offset, spacing, and intensity being characteristics of the cell type. Our group subsequently developed a similar sensor based on electrically injected VECSEL diodes [12]. The active laser-based intracavity spectroscopic biosensors investigated thus far require relatively high gain to overcome the losses associated with the introduction of the fluidic cavity. The high gain requirement in turn necessitates optical pumping or relatively complicated fabrication of electrically injected VECSELs. Thus, this paper is motivated in part by the benefits of a passive cavity interferometric system that retains transverse mode spectrum dependence on cells in a resonator but does not require laser gain media inside the cavity [13]. Instead, transmission spectra are obtained by illuminating the passive cavity system with an external continuum light source such as an LED or a bright incandescent lamp easing the requirements on cavity finesse and loss as well as reducing system cost. Passive cavity-based intracavity spectroscopy is also expected to simplify the analysis of cell-induced transverse mode spectral changes by eliminating the complexities associated with an active laser cavity such as mode confinement factors, material gain, and various losses.

Accordingly, a passive optofluidic intracavity spectrometry proof-of-concept system has been implemented in order to realize real-time label-free detection of single biological cells using optical sensing techniques in a microfluidic environment. Section II describes the structures of the optical sensing system including the microfluidic FP chip, as well as discussing the sensing mechanism for OFIS. The key point is that the transverse mode spectrum of the cell-loaded cavity is determined by the refractive index structure of the cell including its size and shape much as a lens inside an FP cavity alters the transverse mode spectrum. Experimental single-cell spectra obtained using this method are presented in Section III and qualitatively appear to have characteristics such as the number of modes and mode spacing that can be used to differentiate cells. To further evaluate the utility of OFIS, a preliminary method for quantitative calculation of the spectral correlation was developed and evaluated as discussed in Section IV. The results have demonstrated the feasibility of using the approach detailed in this paper to detect certain types of single biological cells, indicating that further work is warranted to develop miniaturized, prototype OFIS systems.

II. Sensing Mechanism and Device Design and Fabrication

A. Sensing Mechanism

Microstructures with spatially dependent refractive index profiles introduced into an FP cavity will perturb the modes of the resonator [14]. In particular, a plane–plane FP cavity containing no internal optical elements ideally only supports a single transverse mode with infinite plane wave behavior. However, a lens or other optical microstructure inserted in the cavity can modify the resonant beam propagation to allow multiple transverse modes at different frequencies.

A simplified example is a single thin lens inside a plane–plane cavity with the resulting transverse mode spectra depending on the cavity length and lens focal length and position according to fundamental optical resonator theory very similar to that discussed by optics or laser texts for curved mirror resonators [15]. For example, the mode spectra for nearly plane–plane, confocal, and concentric resonators have different transverse mode spectra spacing and order. The focal length of the lens in the cavity in turn is a function of the refractive index of the lens and cavity medium and radii of curvature of the lens surfaces. Accordingly, the refractive index profile and size of cells alter the transverse mode spectra of a resonator, providing a sensitive probe of the cells' optical structure. Thus, the specific modal structure is useful in classifying microstructures inside the cavity including differentiating cell types, sizes, and shapes [11]. To first order, the focal power of a cell and thus its dominant effect on transverse mode structure will be determined by the parabolic component of its lateral refractive index variation. Higher order variations in the cell's refractive index profile, analogous to those described by higher order Zernike polynomials for lenses, cause spherical, astigmatic, and other aberrations [16] that will also modify the relative transverse mode frequencies giving additional differentiation. It is theoretically possible that different combinations of cell refractive index, size, and shape could give the same focal length and major aberrations and, thus, the same modal structure. However, this is not expected to be a major issue in many practical situations, and multiple sensor types could be used to resolve such potential interferences. Note that the optical mode diameters are determined by the cell and cavity configuration and are necessarily on the order of the scale of index profile variation in the cell. Thus, the optical mode beams simultaneously interrogate the cell structure as a whole. In the experiments described below, the optical excitation is not externally constrained to sample only small regions within a cell at one time, nor is it scanned within a cell. Accordingly, the effects of the cell nuclei, organelles, and other protein-rich structures that have higher refractive index than the cytoplasm are somewhat averaged by the cell-determined cavity modes.

Even for the idealized case of a uniform index microsphere in a planar cavity, exact solutions of the modes are not known to the authors, although an approximate analysis based on the formulation of the modes as a product of plane wave and spherical

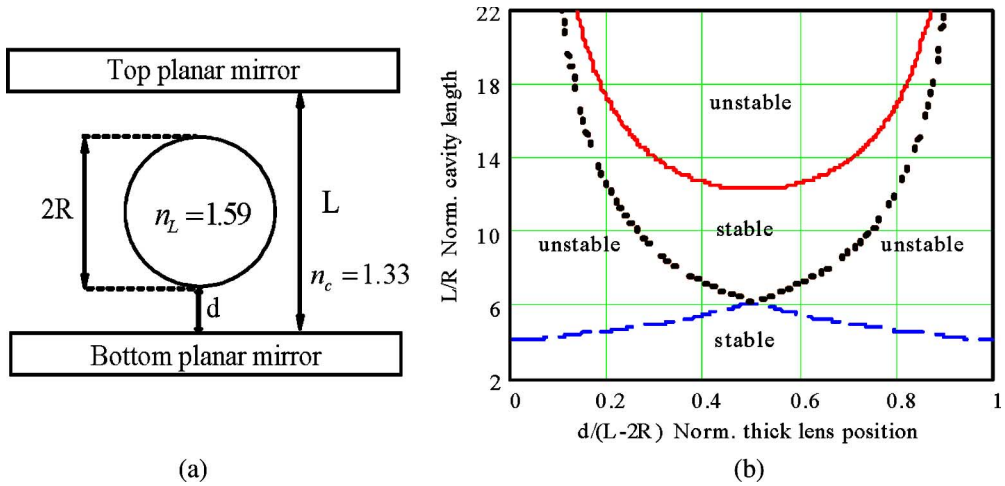

Fig. 1. (a) Schematic diagram of a high-refractive index microsphere in a plane–plane resonator cavity. n_{L} is the refractive index of the microsphere, n_{c} is the refractive index of the microfluidic cavity, d is the distance of the bottom vertex of the sphere from the bottom planar mirror, and L is the microfludic cavity length. (b) Stability diagram for a microsphere in a plane–plane resonator as a function of the normalized resonator configuration coordinate. The left side of the horizontal axis corresponds to sphere at the bottom of the cavity, and the right side corresponds to the sphere close to the top planar mirror.

harmonic solutions applicable to very short cavities has been published [14]. The experimentally observed transverse mode structure of microspheres in this paper is discussed at the end of Section III-A. For the purposes of general design guidelines, an approximate treatment of a microsphere in a plane cavity using paraxial Gaussian beam analysis, which is suitable for a range of cavity lengths, is presented next.

B. Microfluidic Cavity Stability Versus Cavity Length

In this section, classical paraxial Gaussian beam resonator analysis expressed in ABCD matrices is used to set bounds on parameters for resonator stability that are in turn used to guide the sensor design and fabrication process. In order to optimize the sensor response, the microfluidic cavity should be designed to function within the stable range. For simplicity, the cavity described in this section is based on a single polystyrene microsphere with a uniform refractive index of 1.59 submerged in a plane–plane FP resonator filled with water of index 1.33. The microsphere is free to move within the cavity, and the sphere position alters the resonant modes of the cavity. The model cavity geometry is shown schematically in Fig. 1(a).

The stability of an optical resonator can be determined by the magnitude of the trace of the round trip ABCD matrix within the paraxial approximation [15]. The round trip ABCD matrix of the microcavity containing a microsphere is represented as $M_{\mathrm{RT}} = M_{\mathrm{OW1}} \cdot M_{\mathrm{OW2}}$, where M_{OW1} and M_{OW2} represent the one-way (OW) matrix for going from one mirror to the other mirror. Treating the microsphere as a thick ball lens

$$M_{\mathrm{OW1}} = \begin{bmatrix} 1 & \frac{(1-\rho)(L-2R)}{n_{\mathrm{c}}} \\ 0 & 1 \end{bmatrix} \begin{bmatrix} \frac{2n_{\mathrm{c}}-n_{\mathrm{L}}}{n_{\mathrm{L}}} & \frac{2Rn_{\mathrm{c}}}{n_{\mathrm{L}}} \\ \frac{2(n_{\mathrm{c}}-n_{\mathrm{L}})n_{\mathrm{c}}}{Rn_{\mathrm{L}}} & \frac{2n_{\mathrm{c}}-n_{\mathrm{L}}}{n_{\mathrm{L}}} \end{bmatrix} \begin{bmatrix} 1 & \frac{\rho(L-2R)}{n_{\mathrm{c}}} \\ 0 & 1 \end{bmatrix}$$

where the parameter $\rho = d/(L-2R)$ is defined as a normalized fractional distance of the sphere from the first mirror to the vertex of the ball lens d. L is the cavity length, R is the sphere radius, and $n_{\mathrm{c}} = 1.33$ and $n_{\mathrm{L}} = 1.59$ are the refractive indexes of the fluid cavity and the microsphere, respectively. Similarly, the one-way ABCD matrix from the second mirror to the first mirror can be calculated as

$$M_{\mathrm{OW2}} = \begin{bmatrix} 1 & \frac{\rho(L-2R)}{n_{\mathrm{c}}} \\ 0 & 1 \end{bmatrix} \begin{bmatrix} \frac{2n_{\mathrm{c}}-n_{\mathrm{L}}}{n_{\mathrm{L}}} & \frac{2Rn_{\mathrm{c}}}{n_{\mathrm{L}}} \\ \frac{2(n_{\mathrm{c}}-n_{\mathrm{L}})n_{\mathrm{c}}}{Rn_{\mathrm{L}}} & \frac{2n_{\mathrm{c}}-n_{\mathrm{L}}}{n_{\mathrm{L}}} \end{bmatrix} \begin{bmatrix} 1 & \frac{(1-\rho)(L-2R)}{n_{\mathrm{c}}} \\ 0 & 1 \end{bmatrix}.$$

The trace of the round trip ABCD matrix can be readily calculated as a function of the sphere refractive index and position. The stability diagram for a polystyrene sphere placed inside a microfluidic cavity filled with water is shown in Fig. 1(b).

The numerical calculation result in Fig. 1(b) has clearly shown that the cavity length yielding a single point solution is approximately $L = 6.05R$ for the refractive indices used here. Increasing the cavity length past this point starts again expanding the range of stable solutions until a cavity length of $L = 12.3R$ gives a center point stability factor of $\mathrm{Tr}(M_{\mathrm{RT}}) = +1$. Increasing the cavity length past this point will cause the center lens position to be unstable while some intermediate off-center positions are stable, but the positions near the mirrors remain unstable. Increasing the cavity length to very large multiples of the radius then leaves only a decreasing, narrow range of stable lens separations near but not directly against the mirrors. Most importantly, for short cavities of length $L < 4R$, the cavity is stable for all microsphere positions. Therefore, the $10 \sim 30$-μm-deep cavities used in this paper will be unconditionally stable for 10-μm-diameter spheres.

C. Fabrication of Microfluidic FP Cavity in Glass

Glass-based microfluidic devices, especially those coated with reflective thin films inside the etched channels, are very attractive for microcavity spectroscopy because of their good surface rigidity and smoothness that are favorable for making a high-finesse optical cavity. A process based on thermocompressive gold bonding of glass with etched channels has been

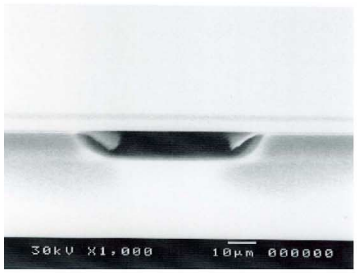

(a)

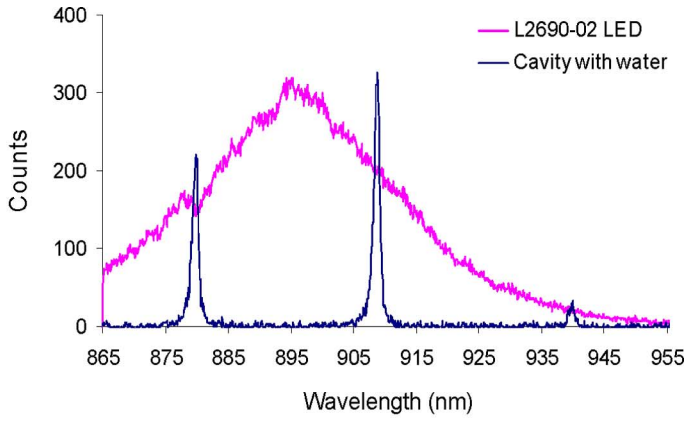

(b)

Fig. 2. (a) SEM picture of a cavity cross section after thermocompressive bonding. (b) Bare microfluidic FP cavity transmission spectrum illuminated with a well-collimated Hamamatsu LED.

developed to fabricate microfluidic FP cavities [17]. The cavities used in the experiments described below were formed by etching $10 \sim 30$-μm-deep and $100 \sim 200$-μm-wide channels in Pyrex glass and coating the surfaces with 35-nm-thick gold layers as the reflectors, which had a calculated power reflectivity of 93% at 890 nm, for the FP cavity. Through holes of 1-mm diameter were drilled at the end of the channel before bonding the glass superstrate and substrate in order to incorporate nanoports onto the sensor chip to overcome the capillary force induced fluid flow by using pressure balancing syringes at the end ports of the channel. After drilling the holes, the superstrate and substrate patterned with the reflectors are joined using a thermocompressive gold-to-gold diffusion bonding technique inside a 350 °C oven in a 10^{-3}-torr vacuum in order to form the FP interferometer. Properties of the microfluidic cavity were characterized by atomic force microscopy (AFM) and optical transmission spectroscopy. A mirror root-mean-square (rms) surface roughness of 1.765 nm was measured by AFM after mirror coating. The FP cavity mirror tilt measured from the transmission spectra at different positions along the channel indicated a mirror tilt of less than 0.1°. Fig. 2 shows a SEM cross section of a 7-μm-deep cavity after the thermocompressive wafer bonding and the optical transmission spectra of a $\sim$25-μm-deep cavity filled with water. The measured cavity finesse of $\sim$30 is in good agreement with the calculations based on the combined effects of the mirror reflectivity, roughness, and tilt, which provides a maximum calculated finesse of 31. Further detailed comparisons are presented in reference [17]. The rigid properties of the glass, strong bonding, and small dimensions result in a very stable FP interferometer as indicated by the good finesse and lack of longitudinal mode drift.

D. Optical Detection System

The prototype OFIS system used for the experiments presented in this paper consisted of a microfluidic chip containing microchannels with mirror coatings to form a FP cavity, an LED illumination source, a customized optical microscope, and a fiber coupled spectrometer. Detection and differentiation of cells are based on the transmission mode spectra of cells in fluid-filled FP cavities and illuminated by an LED, as schematically illustrated in Fig. 3. The LED (Hamamatsu L2690-02) with a full-width at half-maximum of 30 nm and a radiant flux of 18 mW was forward biased at 100 mA. The transmitted light from the fluidic cavity was collected by a 62.5-μm core diameter multimode fiber (MMF) and then analyzed with a 0.3-nm resolution Ocean Optics spectrometer (HR2000).

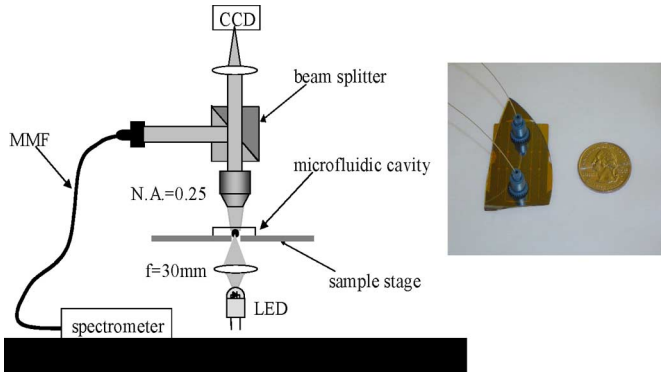

Fig. 3. Customized microscope system used to measure the optical spectrum of the microfluidic FP cavity. The inset shows a top view of the fabricated microfluidic chip fitted with nanoports and tubing for delivering the cell containing fluids from a syringe.

III. Intracavity Spectroscopy

Spectra of different types of polystyrene spheres and biological cells were measured by introducing them into the fluid-filled etched channels. A biconcave lens ($f = 30$ mm) focused the LED light from the bottom to effectively excite the higher order transverse modes of the fluidic cavity. Transmitted light was collected by an MMF through the customized microscope shown in Fig. 3. The focal length of the optical system was adjusted to make the light collection spot size, i.e., the image size of the light collecting fiber's core (approximately 5 to 10 μm in diameter) in order to probe single cells inside the fluidic cavity. The illuminating beam size should be larger than the cell size [18] in order to couple the higher order transverse modes. The fiber can be positioned to simultaneously collect the light from all the transverse modes of one cell by temporarily back-illuminating it and aligning the image of the fiber core to the

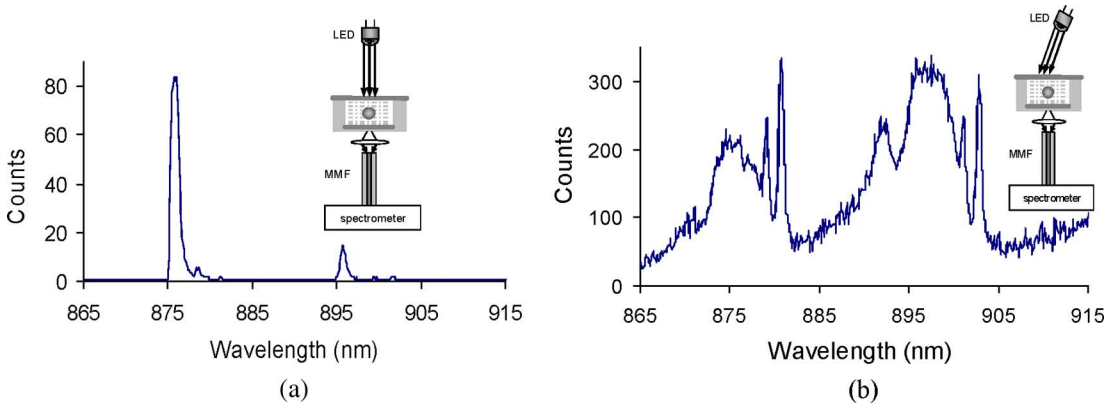

Fig. 4. Transmission spectrum of a single 5-μm-diameter polystyrene sphere with uniform refractive index of 1.59 submerged in deionized water under (a) normal and (b) tilted ($\sim$20° from normal) illumination.

cell to be measured. Since the method uses spectroscopy, i.e., measurement of transverse mode frequencies or corresponding wavelengths, there is no concern about the relatively large MMF not resolving individual regions of a cell, nor is there a need to scan the fiber image within the cell. In order to align the fiber core image to the cell, fluid flow is stopped and thus the cell position is stabilized by balancing the pressure of the two syringes attached to the nanoports at the ends of the channel. No particular apparatus is provided to control the cell orientation in the experiments reported here, although gravity and settling of the cells against the bottom of the channel may affect the orientation of the cells. The stability and repeatability of the spectra reported below indicate that cell orientation was not a major issue. A flowing microfluidic environment may necessitate the use of sheath fluids or other measures to control cell orientation in future work.

A. Transmission Spectra of Polystyrene Spheres

Initial transmission spectra were obtained from the microfluidic cavity filled with a water suspension of polystyrene microspheres (purchased from Bangs Laboratories, Inc.) as they resembled cells but with well controlled size, shape, and index of refraction. Typical transmission spectra for a 5-μm diameter polystyrene sphere under illumination at normal incidence and tilted at approximately 20° are presented in Fig. 4(a) and (b), respectively, together with diagrams showing the mode excitation conditions.

The spectrum in Fig. 4(b) clearly shows additional narrow transmission resonances, corresponding to the transverse cavity modes, compared to the bare cavity modes seen in Fig. 2(b). The cavity's transverse mode groups are repeated three times, corresponding to three longitudinal modes, within the wavelength range of the LED. For each longitudinal mode, there are two broad peaks at lower wavelength and two narrow peaks that are approximately 5 nm longer than the main broad peak. The free spectral range of the 12-μm-deep cavity is $\sim$20 nm, corresponding to the longitudinal mode separation. The number of the transverse modes and the spectral differences of neighboring modes provide useful information about the sphere inside the microfluidic cavity [14]. The broad peak is much stronger than the narrow ones for normal incidence excitation, as shown in Fig. 4(a), while the slightly longer wavelength and narrow peaks are enhanced by off axis illumination shown in Fig. 4(b). Tilted illumination greatly decreases the total transmission, making the spectra appear more noisy at the required longer integration times. As seen below, the narrow peaks are typically stronger for biological cells than for microspheres, perhaps because the higher curvature and index of spheres makes their effective focal length shorter than that of cells.

There is some ambiguity in the assignment of specific transverse mode orders to the various spectral peaks. Because higher order transverse modes are expected to be more strongly excited at higher illumination angles, the narrow peaks are tentatively termed higher order transverse modes, while the slightly lower, broad wavelength peak is taken as the fundamental mode. The same trends with illumination angle and relative mode positions are exhibited for the cases of biological cells presented below. The assumption of mode orders places the higher order modes at longer wavelengths than the fundamental mode, as seen in relatively long concentric resonator cavities [15]. Prior work on microspheres indicated that higher order modes occurred at shorter wavelength than the fundamental mode in relatively short laser cavities that presumably had the same length as the microsphere diameter [14]. That experiment was able to excite single modes near laser threshold, allowing the identification of specific modes by imaging the emission pattern. The use in the present experiments of a broadband continuum source that simultaneously excites multiple transverse and longitudinal modes complicates the determination of the exact mode profile associated with each spectral peak by similar means. However, the use of a tunable laser source or imaging spectrometer should resolve this ambiguity in the future.

B. Transmission Spectra of Single Biological Cells

In the case of real biological cells, the situation is expected to be more complicated because of the unknown refractive index, absorption, orientation, and nonuniformity of cell geometry, but repeatable spectra were still observed. The first biological cell type investigated was yeast (Y) cells because of their ready availability and size (8 to 15 μm in diameter) compatibility with the optical beam dimensions. Transmission spectra for three separate single Y cells prepared in water are shown in Fig. 5

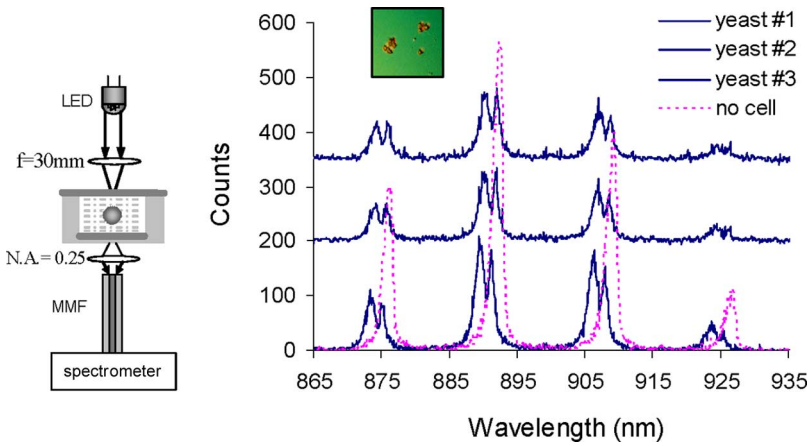

Fig. 5. Transmission spectra of three separate single Y cells. The bare cavity mode spectrum is also shown with the dashed line. The inserted image of the Y cells was taken by a dark field microscope.

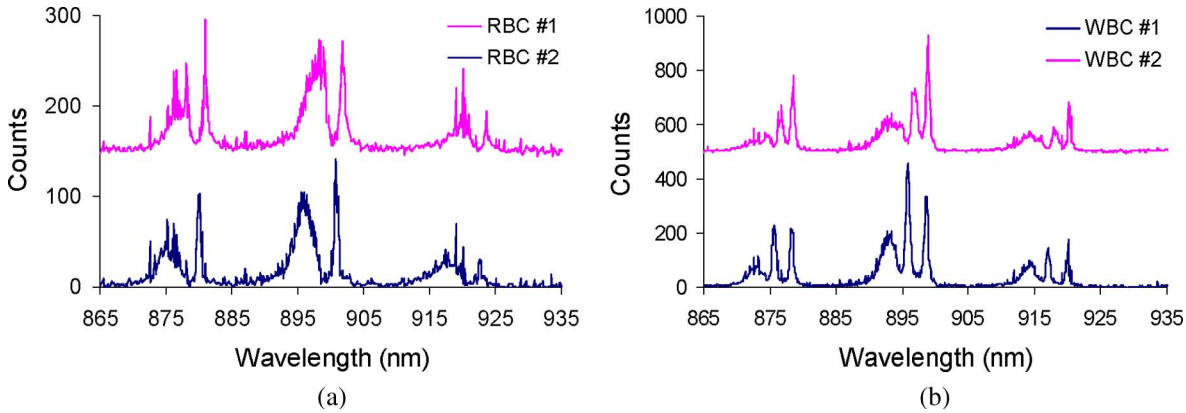

Fig. 6. Transmission spectra of (a) red and (b) white human blood cells. The mode excitation condition is the same as shown in Fig. 5.

and appear relatively similar. The bare cavity mode observed in regions away from the Y cells is also shown with the dashed line. A shift in wavelength is anticipated between the bare cavity mode and even the fundamental optical mode in the presence of a cell both because of a variation in the transverse optical confinement as well as the integrated optical path length changing due to the cell's higher index of refraction compared to the water. Bare cavity regions or specific cells can be interrogated by simply horizontally translating the fiber optic to accept the image of that region. The relative fiber optic position can be determined by backward illuminating the fiber and observing the light spot relative to the cell positions in the microscope. The shift between the cell's fundamental mode and the neighboring bare cavity mode provides information but is not used in the correlation calculations presented in Section IV.

Next, microfludic FP cavity transmission spectra for several blood cells were obtained. The cells were obtained from a single human body and introduced into the microfluidic cavity without any dilution of the original blood serum. Two distinct types of spectra were obtained corresponding to red blood cells (RBCs), as shown in Fig. 6(a), and what are believed to be various types of WBCs, as shown in Fig. 6(b). The spectral signatures of the different cell types are considered to be sufficiently qualitatively unique to differentiate them. The Y cells showed

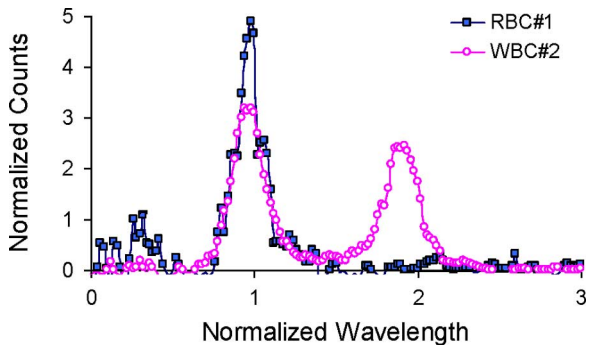

Fig. 7. Spectra of a RBC and a WBC processed according to the steps discussed in the text and ready for a correlation integral.

a single, relatively broad transmission peak at slightly longer wavelength than what is assumed to be the fundamental mode. The blood cells showed strong, narrow transmission peaks with one higher order peak for RBCs and two higher order peaks for WBCs at larger wavelength offsets. The amount of offset varies somewhat from cell to cell and may be associated with cell size. Further quantitative cross correlation analysis of the cell spectra will be presented in Section IV.

Different biological cell's spectra exhibited variations in peak amplitude, mode spacing, and number of higher order

TABLE I
CORRELATION COEFFICIENT OF SPECTRA FOR RBC, WBC, AND Y CELLS

	RBC1	RBC2	RBC3	RBC4	WBC1	WBC2	Y1	Y2	Y3
RBC1	1	0.84	0.84	0.8721	0.7016	0.6716	0.8430	0.862	0.7993
RBC2	0.84	1	0.9011	0.847	0.757	0.7442	0.820	0.8115	0.8666
RBC3	0.8721	0.9011	1	0.8784	0.7026	0.7241	0.6810	0.7660	0.7314
RBC4	0.9252	0.847	0.8784	1	0.7591	0.7223	0.9068	0.9230	0.8907
WBC1	0.7016	0.757	0.7026	0.7591	1	0.6507	0.6910	0.7690	0.7533
WBC2	0.6716	0.7442	0.7241	0.7223	0.6507	1	0.571	0.6385	0.7465
Y1	0.843	0.820	0.6810	0.9068	0.6910	0.571	1	0.9699	0.8707
Y2	0.862	0.8115	0.7660	0.9230	0.7690	0.6385	0.9699	1	0.9247
Y3	0.7993	0.8666	0.7314	0.8907	0.7533	0.7465	0.8707	0.9247	1

transverse modes. All of these spectral differences are attributed to the optical confinement perturbation inside the microfluidic FP cavity. Although some variation in the cell spectra might be expected based on exact organelle positions or movement, the observed spectra were stable and repeatable during the experiments. Further work is needed to understand in detail the effect of organelle position or size variation on transverse spectra. Theoretical modeling of the modal structures of the cell-loaded microfluidic using finite-difference time-domain simulations is in progress and will be reported elsewhere.

IV. CORRELATION ANALYSIS OF BIOLOGICAL CELL SPECTRA

In order to prove the repeatability and reliability of the biosensor to differentiate single biological cells, transmission spectra of multiple cells of each type used in this paper have been taken repeatedly. While the spectra corresponding to a particular cell type are qualitatively considered to be repeatable, it is useful to quantitatively assess the similarities of the spectra. Correlation analysis is a widely used technique in biochemical experiments to recognize specific chemical components [19], [20] and will be applied here to cell differentiation.

The spectral data were prepared for correlation computations using the following steps. 1) A portion of each spectrum corresponding to a single free spectral range of the cavity was selected. Typically, this was the central, highest intensity portion of the spectra. 2) The fundamental mode peak, which is taken taken to be the broad, lowest wavelength peak, was assigned a relative wavelength offset of 0 nm. 3) The wavelength offset range was normalized to place the dominate peak of each spectra at the same point. 4) A Lorentzian lineshape curve was fit to the fundamental mode and subtracted from the spectrum, thus removing the fundamental, which was taken to contain no cell specific information. 5) Last, the rms amplitude of the net spectrum containing the transverse mode transmission peaks was normalized to unity. The resulting spectra for one RBC and one WBC are shown in Fig. 7 as examples.

The correlation coefficients between the transmission spectra of four RBCs, two WBCs, and three Y cells were then computed and recorded in Table I. The correlation data shows that the RBCs can be differentiated from the other blood cells based on a correlation coefficient threshold of 0.8 but that the current method is not sufficient to differentiate RBCs from Y cells, although this interference has limited practical significance. It is also noteworthy that the two WBC spectra had a relatively low correlation and may have come from different cell types, e.g., neurophils and lymphocytes. The results presented here were initial correlation studies, and better results are expected from more complete studies, including the creation of correlation templates or masks that account for the variability of spectra for the same type of cells.

V. CONCLUSION

In this paper, a passive cavity microfluidic system on glass substrates was developed as a test bed for OFIS of single polystyrene beads and single biological cells. Transmission spectra for a FP cavity containing polystyrene spheres, Y cells, human RBCs, and WBCs were obtained using tilted illumination to enhance transverse mode structure. The transmission spectra for the cell types are qualitatively different in terms of the number, relative position, and relative wavelength offset of transverse modes. Preliminary quantitative correlation analysis of the spectra demonstrates the capability of the biosensor to differentiate certain pairs of single biological cells. Thus, the approach described in this paper may be extended to detect other types of cells and provide a useful label-free optical technique for recognizing cells in a microfluidic environment.

ACKNOWLEDGMENT

The authors would like to thank Dr. S. A. Feld for technical assistance with fabrication, X. Chen for providing cells, and B. Pownall for assistance with figure preparation.

REFERENCES

[1] J. Beuthan, O. Minet, J. Helfmann, M. Herrig, and G. Muller, "The spatial variation of the refractive index in biological cells," *Phys. Med. Biol.*, vol. 41, no. 3, pp. 369–382, 1996.

[2] V. Backman, M. B. Wallace, L. T. Arendt *et al.*,"Detection of preinvasive cancer cells," *Nature*, vol. 406, no. 6791, pp. 35–36, Jul. 2000.

[3] J. Emmelkamp, F. Wolbers, H. Andersson, R. S. DaCosta, B. C. Wilson, I. Vermes, and A. V. D. Berg, "The potential of auto fluorescence for the detection of single living cells for label-free cell sorting in microfluidic systems," *Electrophoresis*, vol. 25, no. 21/22, pp. 3740–3745, Nov. 2004.

[4] A. C. Romano, E. M. Espana, S. H. Yoo, M. T. Budak, J. M. Wolosin, and S. C. G. Tseng, "Different cell sizes in human limbal and central corneal basal epithelia measured by confocal microscopy and flow cytometry," *Investig. Ophthalmol. Vis. Sci.*, vol. 44, no. 12, pp. 5125–5129, 2003.

[5] C. G. Xie and Y. Q. Li, "Confocal micro-Raman spectroscopy of single biological cells using optical trapping and shifted excitation difference techniques," *J. Appl. Phys.*, vol. 93, no. 5, pp. 2982–2986, Mar. 2003.

[6] R. S. Gurajar, V. Backman, L. T. Perelman, I. Georgakoudi *et al.*, "Imaging human epithelial properties with polarized light scattering spectroscopy," *Nat. Med.*, vol. 7, no. 11, pp. 1245–1248, 2001.

[7] P. B. Tarsa, A. D. Wist, P. Rabinowitz, and K. K. Lehmann, "Single-cell detection by cavity ring-down spectroscopy," *Appl. Phys. Lett.*, vol. 85, no. 19, pp. 4523–4525, Nov. 2004.
[8] A. Katz, A. Alimova, M. Xu, E. Rudolph, M. K. Shah, H. E. Savage, R. B. Rosen, S. A. McCormick, and R. R. Alfano, "Bacteria size determination by elastic light scattering," *IEEE J. Sel. Topics Quantum Electron.*, vol. 9, no. 2, pp. 277–287, Mar./Apr. 2003.
[9] X. J. Liang, A. Q. Liu, X. M. Zhang, P. H. Yap, T. C. Ayi, and H. S. Yoon, "Determination of refractive index of single living cell using integrated biochip," in *Proc. 13th Int. Conf. Solid-State Sens., Actuators, Microsyst.*, 2005, pp. 1712–1715.
[10] Y. Zhang, K. L. Cooper, and A. B. Wang, "Multicavity Fabry–Perot interferometric thin-film sensor with built-in temperature compensation," *IEEE Photon. Technol. Lett.*, vol. 17, no. 12, pp. 2712–2714, Dec. 2005.
[11] P. L. Gourley, "Biocavity laser for high-speed cell and tumor biology," *J. Appl. Phys. D*, vol. 36, no. 14, pp. R228–R239, 2003.
[12] D. Kumar, H. Shao, and K. L. Lear, "Microfluidic cavity surface emitting laser based biosensor," in *Proc. 17th Annu. Meeting IEEE LEOS*, Nov. 2004, vol. 1, pp. 118–119.
[13] H. Shao, D. Kumar, S. A. Feld, and K. L. Lear, "Micro-fluidic passive cavity interferometer based biosensor," in *Proc. 17th Annu. Meeting IEEE LEOS*, Nov. 2004, vol. 1, pp. 120–121.
[14] K. E. Meissner, P. L. Gourley, T. M. Brennan, B. E. Hammons, and A. E. McDonald, "Intracavity spectroscopy in vertical cavity surface-emitting lasers for micro-optical-mechanical systems," *Appl. Phys. Lett.*, vol. 69, no. 11, pp. 1517–1519, Sep. 1996.
[15] A. E. Siegman, *Lasers*. Mill Valley, CA: Univ. Sci., 1986, ch. 19 and 21.
[16] G. Smith, B. K. Pierscionek, and D. A. Atchison, "The optical modeling of the human lens," *Ophthalmic Physiol. Opt.*, vol. 11, no. 4, pp. 359–369, Oct. 1991.
[17] H. Shao, D. Kumar, S. A. Feld, and K. L. Lear, "Fabrication of a Fabry–Perot cavity in a microfluidic channel using thermocompressive gold bonding of glass substrates," *J. Microelectromech. Syst.*, vol. 14, no. 4, pp. 756–762, Aug. 2005.
[18] T. Klaassen, J. D. Jong, M. V. Exter, and J. P. Woerdman, "Transverse mode coupling in an optical resonator," *Opt. Lett.*, vol. 30, no. 15, pp. 1959–1961, Aug. 2005.
[19] E. Gratton, S. Breusegem, N. Barry, Q. Ruan, and J. Eid, "Fluctuation correlation spectroscopy in cells: Determination of molecular aggregation," in *Biophotonics-Optical Science and Engineering for the 21st Century*. Norwell, MA: Kluwer, 2004.
[20] P. Schwille, F. J. MeyerAlmes, and R. Rigler, "Dual-color fluorescence cross-correlation spectroscopy for multicomponent diffusional analysis in solution," *Biophys J.*, vol. 72, no. 4, pp. 1878–1886, Apr. 1997.

Hua Shao (S'04) received the B.S.E.E. and M.S. degrees in physics from Nanjing University of Science and Technology, Nanjing, China, in 1998 and 2001, respectively. She is currently working toward the Ph.D. degree with the Electrical and Computer Engineering Department, Colorado State University, Fort Collins.

Her research interests include the design and fabrication of photonic biosensors and numerical modeling of optical waveguides.

Dhiraj Kumar (S'03) received the B.E. degree in electronics and telecommunications engineering from Pt. Ravi Shankar Shukla University, Raipur, India, in 2002 and the M.S.E.E. degree from Colorado State University, Fort Collins, in 2005.

He is currently working as an Optoelectronic Device Engineer at Opticomp Corporation, Zephyr Cove, Nevada.

Kevin L. Lear (SM'88–M'90) received the B.S.E.E. degree from the University of Colorado, Boulder, in 1984 and the M.S.E.E. and Ph.D.E.E. degrees from Stanford University, Stanford, CA, in 1985, and 1990, respectively.

He was a Senior Member of Technical Staff at Sandia National Laboratories, Albuquerque, NM, from 1990 to 1997. In 1997, he became the Chief Scientific Officer at Micro Optical Devices, Inc., Albuquerque: a small business commercializing VCSELs, which was subsequently acquired by Emcore Corporation. In 1999, he joined Colorado State University, Fort Collins, as the Rockwell Anderson Associate Professor of Electrical and Computer Engineering. His research is currently focused on photonic biosensors and components and systems for high-speed optical communication.

Dr. Lear received an IEEE Lasers and Electro-Optics Society Distinguished Lecturer Award in 1996 for his work on VCSELs.